JOURNAL OF CATALYSIS 134, 445–468 (1992)

A Kinetic Model of the Water Gas Shift Reaction

C. V. OVESEN,* P. STOLTZE,* J. K. NØRSKOV,* AND C. T. CAMPBELL†

*Laboratory of Applied Physics, Technical University of Denmark, DK-2800 Lyngby, Denmark, and †Chemistry Department, University of Washington, Seattle, Washington 98195

Received April 16, 1991; revised July 25, 1991

A kinetic model of the water gas shift reaction based on a description of its elementary steps at the atomic level is presented. Input data for elementary steps are taken from available single crystal studies. The model is successfully tested against kinetic data for a working Cu-based catalyst. Expressions are derived for the activation energy and reaction orders. © 1992 Academic Press, Inc.

1. INTRODUCTION

The *water gas shift (WGS) reaction*

$$CO + H_2O \rightleftharpoons CO_2 + H_2 \qquad (1)$$

is an important step in the production of H_2 in a number of chemical processes (*1*). This reaction is performed in industry over a range of reaction conditions. Different catalyst formulations are used depending on the reaction conditions. The high-temperature shift reaction is performed at 590–720 K using a catalyst based on iron oxide (*2, 3*), while the low-temperature shift reaction is performed at 470–520 K using a (Cu,Zn,Al)-based catalyst (*3*). The structure of this catalyst, as well as its reaction mechanism, remains controversial (*1*). The simplest possibility is that the active structure is the basal planes of metallic copper (*4–7*). The simplest possible reaction mechanism is that the intermediates found on the surface of the working catalyst are limited to the reactants and their dissociation products (*4*). In this paper we investigate whether a simple reaction mechanism coupled with input data for Cu single crystals gives a reasonable description of the WGS reaction for a working Cu-based catalyst.

In Sections 2 and 3 we derive a kinetic model based on the available knowledge on the adsorption and reaction of CO, CO_2, H_2, and H_2O on single crystals of copper. In Section 4 we provide equations for the calculation of thermodynamic properties of the reactants and intermediates based on their spectroscopic properties. In Section 5 we discuss a number of data calculated from the model, we use the model to investigate the origin of the activation energy and the reaction orders for the catalytic reaction, and we examine two limiting cases of the model. In Section 6 we compare calculated and experimental data (*8, 9*) for the water gas shift reaction for a catalyst operating at 1 atm. This leads to a critical discussion of the input parameters in Section 7. We discuss the determination of input parameters from available experimental data in detail in Appendix A, and in Appendix B we outline the derivation of some of the equations from Sections 3 and 4 and Appendix A.

The purpose of our studies is not to present a kinetic model which will reproduce one or a few of the aspects of water gas shift reaction very accurately. The point we make is that a physically reasonable treatment of the proposed reaction mechanism (*4*) with kinetic and thermodynamic data measured for Cu single crystals leads to a reasonably accurate description of most aspects of the observed kinetics.

2. REACTION MECHANISM

Over the years a very large number of studies of the adsorption of small molecules on copper single crystals have been made.

0021-9517/92 $3.00

TABLE 1

Elementary Steps in the Redox Mechanism for the Water Gas Shift Reaction

Reaction steps	Number
$H_2O(g) + * \rightleftharpoons H_2O*$	1
$H_2O* + * \rightleftharpoons OH* + H*$	2
$2OH* \rightleftharpoons H_2O* + O*$	3
$OH* + * \rightleftharpoons O* + H*$	4
$2H* \rightleftharpoons H_2(g) + 2*$	5
$CO(g) + * \rightleftharpoons CO*$	6
$CO* + O* \rightleftharpoons CO_2* + *$	7
$CO_2* \rightleftharpoons CO_2(g) + *$	8

Note. In the reaction sequence * is a surface site and $X*$ is the molecule X adsorbed on a site.

Recently, the rate of the shift reaction has been measured on single crystals of Cu (*4, 10*). From these studies it was concluded that the reaction mechanism for the water gas shift reaction can be described by eight elementary steps (*4*) as listed in Table 1. This reaction mechanism is commonly known as the *redox mechanism*. The existence of more complicated species, such as formate (*8, 11, 12*), is excluded in this mechanism. The redox mechanism appears to be the simplest mechanism that can account for the reaction steps observed on single crystal surfaces. As we show in the following this reaction mechanism already has a rather complicated kinetics. For these reasons we think this mechanism and its kinetics deserve a thorough study before more complicated mechanisms are examined. In the following we investigate those aspects of the redox mechanism that are relevant for the reaction at low pressures.

A comparison of the rate of dissociation of water to the rate of the water gas shift reaction in a H_2O + CO atmosphere over single-crystal surfaces of Cu indicates that the dissociation of H_2O, reaction step 2, is rate-limiting under these conditions (*4*). However, if the CO/H_2O ratio is sufficiently low, the reaction between CO and adsorbed oxygen, step 7, must become rate-limiting. For the reverse water gas shift reaction this step has been suggested to be rate-limiting (*13*). Under the reverse shift condition, water is formed through reaction steps 3 and 4 while reaction step 2 has a negligible rate. It has been suggested that reaction step 4, the formation of OH*, is rate-limiting when water is formed by reduction of surface oxide (*14*). Therefore, in the derivation of the kinetic expression we assume that both the dissociation of H_2O*, reaction step 2 or step 4, and the reaction between CO* and O*, reaction step 7, may be slow. We discuss the theoretical aspects of the changes in rate-limiting step and how these changes are reflected in the experimental data in Sections 5 and 6. We also show in Section 6 that under forward shift conditions the rate of step 4 is negligible and the reaction proceeds through step 2 and step 3.

One might attack the reaction sequence in Table 1 by writing kinetic equation for all steps and solving the equations numerically using large, guessed rate constants for the fast steps. However, we prefer to use equilibrium equations for the slow steps as this simplifies the problem sufficiently to allow analytical solution for the rate and coverages. Even if the analysis in our approach is initially much harder, it does lead to an understanding of the origin of the macroscopic kinetics, Section 5, that would be very difficult to obtain in a purely numerical approach.

3. KINETIC EQUATIONS

Since reaction steps 2, 4, and 7 may all be rate-limiting we obtain the following set of rate and equilibrium equations:

$$K_1 \frac{p_{H_2O}}{p_0} \theta_* = \theta_{H_2O*} \tag{2}$$

$$r_2 = k_2 \theta_{H_2O*} \theta_* - \frac{k_2}{K_2} \theta_{OH*} \theta_{H*} \tag{3}$$

$$K_3 \theta_{OH*}^2 = \theta_{H_2O*} \theta_{O*} \tag{4}$$

$$r_4 = k_4 \theta_{OH*} \theta_* - \frac{k_4}{K_4} \theta_{O*} \theta_{H*} \tag{5}$$

$$K_5\theta_{H*}^2 = \frac{p_{H_2}}{p_0}\theta_*^2 \tag{6}$$

$$K_6\frac{p_{CO}}{p_0}\theta_* = \theta_{CO*} \tag{7}$$

$$r_7 = k_7\theta_{CO*}\theta_{O*} - \frac{k_7}{K_7}\theta_{CO_2*}\theta_* \tag{8}$$

$$K_8\theta_{CO_2*} = \frac{p_{CO_2}}{p_0}\theta_*. \tag{9}$$

In these equations, K_1 to K_8 are the equilibrium constants of reaction steps 1–8 and p_0 is the thermodynamic reference pressure. In Section 4 we will return to the calculation of the equilibrium constants from the molecular partition functions. K_g is the equilibrium constant for the gas phase equilibrium; as discussed in Appendix B, it is related to the equilibrium constants K_1 to K_8 by

$$K_g = K_1K_2^{3/2}K_3^{1/2}K_4^{1/2}K_5K_6K_7K_8. \tag{10}$$

k_2, k_4 and k_7 are rate constants for reaction steps 2, 4, and 7. We assume that k_2, k_4, and k_7 have Arrhenius form,

$$k_2 = A_2\exp\left(-\frac{E_2^\ddagger}{k_BT}\right) \tag{11}$$

$$k_4 = A_4\exp\left(-\frac{E_4^\ddagger}{k_BT}\right) \tag{12}$$

$$k_7 = A_7\exp\left(-\frac{E_7^\ddagger}{k_BT}\right), \tag{13}$$

where k_B is Boltzmann's constant. In Appendix A we determine A_2, A_4, A_7, $E_2^\ddagger$, $E_4^\ddagger$, and $E_7^\ddagger$ from experimental data.

In addition to the reaction equations steps 1–8, mass balances for OH* and O* show that the following relation exists between the rates of reaction steps 2, 4, and 7 and the net rate for the water gas shift reaction for a catalyst operating in a stationary state:

$$r = \tfrac{1}{2}(r_2 + r_4) = r_7. \tag{14}$$

This equation is derived in Appendix B. Finally, a site must either be free or occupied by one of the intermediates,

$$\theta_* + \theta_{H_2O*} + \theta_{OH*} + \theta_{O*} + \theta_{H*} + \theta_{CO*} + \theta_{CO_2*} = 1. \tag{15}$$

The number of sites is constant and the competition for the adsorption sites has important consequences for the macroscopic kinetics. This is the reason for treating the surface sites as if they were a reactant in the reaction equations.

The system of Eqs. (2)–(8) and (10)–(15) leads to a unique and explicit solution for the coverage of each species,

$$\theta_*^{-1} = 1 + K_1\frac{p_{H_2O}}{p_0} + \left(\frac{K_1}{K_3}\frac{p_{H_2O}}{p_0}\right)^{1/2}\left(\frac{-b + (b^2 + 4ac)^{1/2}}{2a}\right) + \left(\frac{1}{K_5}\frac{p_{H_2}}{p_0}\right)^{1/2} + K_6\frac{p_{CO}}{p_0} + \left(\frac{-b + (b^2 + 4ac)^{1/2}}{2a}\right)^2 + \frac{1}{K_8}\frac{p_{CO_2}}{p_0} \tag{16}$$

$$\theta_{H_2O*} = K_1\frac{p_{H_2O}}{p_0}\theta_* \tag{17}$$

$$\theta_{H*} = \left(\frac{1}{K_5}\frac{p_{H_2}}{p_0}\right)^{1/2}\theta_* \tag{18}$$

$$\theta_{CO*} = K_6\frac{p_{CO}}{p_0}\theta_* \tag{19}$$

$$\theta_{CO_2*} = \frac{1}{K_8}\frac{p_{CO_2}}{p_0}\theta_* \tag{20}$$

$$\theta_{O*} = \left(\frac{-b + (b^2 + 4ac)^{1/2}}{2a}\right)^2\theta_* \tag{21}$$

$$\theta_{OH*} = \left(\frac{1}{K_3}K_1\frac{p_{H_2O}}{p_0}\theta_*\theta_{O*}\right)^{1/2}, \tag{22}$$

where we have introduced the shorthand notation

$$a = k_7K_6\frac{p_{CO}}{p_0} + \frac{1}{2}\frac{k_4}{K_4}\left(\frac{1}{K_5}\frac{p_{H_2}}{p_0}\right)^{1/2} \tag{23}$$

$$b = \frac{1}{2}\left(\frac{K_1}{K_3}\right)^{1/2}\left(\frac{p_{H_2O}}{p_0}\right)^{1/2} \times \left(\frac{k_2}{K_2}\left(\frac{1}{K_5}\frac{p_{H_2}}{p_0}\right)^{1/2} - k_4\right) \quad (24)$$

$$c = \frac{1}{2}k_2K_1\frac{p_{H_2O}}{p_0} + \frac{k_7}{K_7K_8}\frac{p_{CO_2}}{p_0}. \quad (25)$$

The solution for the net rate of the overall reaction is

$$r = k_7\theta_{CO*}\theta_{O*} - \frac{k_7}{K_7}\theta_{CO_2}\theta_* \quad (26)$$

$$r = \frac{1}{2}\left(k_2\theta_{H_2O}\theta_* - \frac{k_2}{K_2}\theta_{OH*}\theta_{H*} + k_4\theta_{OH*}\theta_* - \frac{k_4}{K_4}\theta_{O*}\theta_{H*}\right). \quad (27)$$

4. THERMODYNAMICS

The equilibrium constants can be calculated from the partition functions of the intermediates. We will assume that all sites are identical and that there is no interaction between adsorbed species except, of course, that only one molecule at a time can adsorb on a site. If interactions between adsorbed species exist but do not vary much with coverage, they will be hard to observe and will be implicitly and approximately included in the calculations. Using these approximations the molecular partition function will factorize into one term for each degree of freedom in the molecule:

$$z = z_t z_u z_r z_e. \quad (28)$$

In the following we use the symmetry of the molecules to determine the number and kinds of the mechanical degrees of freedom. In the determination of the symmetry of the adsorbates, we assume that the surface is structureless; e.g., the symmetry of H_2O* is C_{2v} independent of the crystallographic structure of the surface. This approximation works as we restrict our calculation to low-index surfaces.

The translational partition function, z_t, for a gas molecule is

$$z_t = \left(\frac{2\pi m k_B T}{h^2}\right)^{2/3} \times \frac{k_B T}{p_0}, \quad (29)$$

where m is the mass of a molecule in a container with a pressure p_0 and h is Planck's constant. Equation (29) has been written for the case of triple degeneracy. This will be the case for all gas molecules considered here. The translational partition function at some pressure, p, can be calculated from z_t as

$$z_t(p) = z_t\left(\frac{p_0}{p}\right). \quad (30)$$

The calculation of the partition function at the thermodynamic reference pressure is computationally convenient (*15*).

For adsorbed molecules we will assume that there is no translation, but that the molecule is vibrating parallel and orthogonal to the surface. In the case of the vibration in plane, we will assume double degeneracy unless otherwise is stated. The partition function for this frustrated translation is

$$z_t = \frac{\exp(-(1/2)h\omega_\perp/k_BT)}{1 - \exp(-h\omega_\perp/k_BT)} \times \frac{\exp(-\omega_\parallel/k_BT)}{(1 - \exp(-h\omega_\parallel/k_BT))^2}, \quad (31)$$

where $\omega_\perp$ is the vibration frequency for the singly degenerate vibration orthogonal to the surface and $\omega_\parallel$ is the vibration frequency for the doubly degenerate vibration parallel to the surface.

In some cases no values for the frequency of the parallel frustrated translation are available. In these cases we assume that the molecule is vibrating in a sinusoidal potential,

$$V(x) = V_0\sin\left(\frac{2\pi}{a}x\right). \quad (32)$$

From the lattice constant and an estimate of the depth, V_0, of the potential, the vibration frequency can be estimated.

The vibrational partition function, z_v, consists of a contribution

$$z_v = \frac{\exp(-(1/2)h\omega/k_BT)}{1 - \exp(-h\omega/k_BT)}, \quad (33)$$

where ω is the vibration frequency from each vibrational degree of freedom.

The rotational partition function, z_r, for a linear molecule is

$$z_r = \frac{1}{\sigma}\sum_{j=0}^{\infty}(2j+1)\exp\left(-j(j+1)\frac{B}{k_BT}\right), \quad (34)$$

where σ is the symmetry number and B the rotational constant. For an asymmetrical molecule, the rotational partition function, z_r, may be approximated by (*16*)

$$z_r = \frac{\pi^{1/2}(k_BT)^{3/2}(I_AI_BI_C)^{1/2}}{\sigma\hbar^3}, \quad (35)$$

where σ is again the symmetry number and I_A, I_B, and I_C are the moments of inertia.

The ground state partition function z_e is

$$z_e = \exp\left(-\frac{E_e}{k_BT}\right) \quad (36)$$

where E_e is the energy of the ground state of the molecule. E_e is of electronic origin and measures the stability of the molecule. To extract reaction enthalpies the difference in E_e between reactants and products must be corrected with the difference in thermal energy stored in the mechanical degrees of freedom at the reaction temperature.

The equilibrium constants in the model may easily be calculated from the partition functions:

$$K_1 = \frac{z_{H_2O*}}{z_{H_2O}} \quad (37)$$

$$K_2 = \frac{z_{OH*}z_{H*}}{z_{H_2O*}} \quad (38)$$

$$K_3 = \frac{z_{H_2O*}z_{O*}}{z_{OH*}^2} \quad (39)$$

$$K_4 = \frac{z_{O*}z_{H*}}{z_{OH*}} \quad (40)$$

$$K_5 = \frac{z_{H_2}}{z_{H*}^2} \quad (41)$$

$$K_6 = \frac{z_{CO*}}{z_{CO}} \quad (42)$$

$$K_7 = \frac{z_{CO_2*}}{z_{CO*}z_{O*}} \quad (43)$$

$$K_8 = \frac{z_{CO_2}}{z_{CO_2*}}. \quad (44)$$

Implicit in these equations is the assumption that at most one molecule can adsorb at a site at a time, and that this is the only adsorbate–adsorbate interaction in the system. However, if other types of interactions, such as dipole–dipole interactions or adsorbate-induced reconstructions, are present the adsorbate–adsorbate interaction energy will be adsorbed in the E_e-terms. One may thus view the E_e-terms as *effective* ground state energies.

The number of parameters in the model is large. One could suspect (*15*) that only a few parameters are critical, but we cannot know *a priori* which. Rather than trying to determine this at an early state we concentrate on the determination of reasonable values for all parameters. When this has been done, we can test the model, Section 5, against independent experimental data and we can perform a proper sensitivity analysis for the input parameters, Section 7. We then backtrack and concentrate on the determination of accurate values for the critical parameters. The advantage of this iterative scheme is that a much more complete sensitivity analysis can be made on the full model compared to an analysis for a model where some parameters have been eliminated at an early state.

5. DISCUSSION

Before we proceed to the comparison between experimental and calculated data in the next section, it will be useful to investigate some of the more general aspects of the model. The parameters used in the calcula-

TABLE 2

Table of Thermodynamic Data Used in the Computations

H_2(g)	$\omega = 4405.3\ cm^{-1}$, $B = 60.8\ cm^{-1}$, $\sigma = 2$, $E_e = -35\ kJ\ mol^{-1}$
H*/Cu(111)	$\omega_\perp = 1291\ cm^{-1}$, $\omega_\parallel = 157\ cm^{-1}$, $E_e = -27\ kJ\ mol^{-1}$
H_2O(g)	$\omega_1 = 1594.6\ cm^{-1}$, $\omega_2 = 3657.1\ cm^{-1}$, $\omega_3 = 3755.8\ cm^{-1}$, $\sigma = 2$, $I_A I_B I_C = 5.7658 \times 10^{-141}\ kg^3\ m^6$, $E_e = -306\ kJ\ mol^{-1}$
H_2O*/Cu(111)	$\omega_1 = 1600\ cm^{-1}$, $\omega_2 = 3370\ cm^{-1}$, $\omega_3 = 3370\ cm^{-1}$, $\omega_4 = 745\ cm^{-1}$, $\omega_\perp = 460\ cm^{-1}$, $\omega_\parallel = 21\ cm^{-1}$, $E_e = -359\ kJ\ mol^{-1}$
H_2O*/Cu(110)	$\omega_1 = 1600\ cm^{-1}$, $\omega_2 = 3370\ cm^{-1}$, $\omega_3 = 3370\ cm^{-1}$, $\omega_4 = 745\ cm^{-1}$, $\omega_\perp = 460\ cm^{-1}$, $\omega_\parallel = 21\ cm^{-1}$, $E_e = -365\ kJ\ mol^{-1}$
O*/Cu(110)	$\omega_\perp = 391\ cm^{-1}$, $\omega_\parallel = 508\ cm^{-1}$, $E_e = -243\ kJ\ mol^{-1}$
OH*/Cu(110)	$\omega = 3380\ cm^{-1}$, $\omega_\perp = 280\ cm^{-1}$, $\omega_\parallel = 670\ cm^{-1}$, $E_e = -319\ kJ\ mol^{-1}$
CO(g)	$\omega = 2169.5\ cm^{-1}$, $B = 1.9\ cm^{-1}$, $\sigma = 1$, $E_e = -130\ kJ\ mol^{-1}$
CO*/Cu(111)	$\omega = 2077\ cm^{-1}$, $\omega_\perp = 330\ cm^{-1}$, $\omega_\parallel = 17\ cm^{-1}$, $E_e = -181\ kJ\ mol^{-1}$
CO*/Cu(110)	$\omega = 2088\ cm^{-1}$, $\omega_\perp = 342\ cm^{-1}$, $\omega_\parallel = 17\ cm^{-1}$, $E_e = -190\ kJ\ mol^{-1}$
CO_2(g)	$\omega_1 = 1342.9\ cm^{-1}$, $\omega_2 = 667.3\ cm^{-1}$, $\omega_3 = 2349.3\ cm^{-1}$, $B = 0.39\ cm^{-1}$, $\sigma = 2$, $E_e = -431\ kJ\ mol^{-1}$
CO_2*/Cu(111)	$\omega_1 = 1343\ cm^{-1}$, $\omega_2 = 667\ cm^{-1}$, $\omega_3 = 2349\ cm^{-1}$, $\omega_\perp = 410\ cm^{-1}$, $\omega_\parallel = 14\ cm^{-1}$, $E_e = -463\ kJ\ mol^{-1}$

Note. The details of the determination of these parameters are discussed in Appendix A.

tions are listed in Tables 2 and 3 and the determination of the parameters is discussed in details in appendix A. For the discussion in the present section it will be sufficient to note that the parameters have been chosen to reproduce the thermodynamics of the individual reaction steps as well as the kinetics of the slow steps over single crystal surfaces. The reaction is structure sensitive and for a number of reaction steps the parameters for the reaction over Cu(110) and Cu(111) will be different.

5.1. *Analysis of the Model*

The general set of equations for coverages and rates is very large. However, in principle it is not difficult to incorporate these equations into a computer program. The results we will show in the following have been computed from the general set of equations. Once the full computation has demonstrated the relative importance of each of the reactions step 2, step 4, and step 7 under a given set of conditions, one can introduce approximations, which may greatly simplify the computations for a given set of reaction conditions. In the end of this section we discuss two limiting cases relevant for the forward shift reaction.

TABLE 3

Table of Kinetic Data Used in the Computations

k_2	Cu(111)	$A_2 = 9.90 \times 10^{13}\ s^{-1}$, $E_2^\ddagger = 114.0\ kJ\ mol^{-1}$
k_2	Cu(110)	$A_2 = 1.10 \times 10^{12}\ s^{-1}$, $E_2^\ddagger = 93.3\ kJ\ mol^{-1}$
k_7	Cu(111)	$A_7 = 3.4 \times 10^{12}\ s^{-1}$, $E_7^\ddagger = 64\ kJ\ mol^{-1}$
k_7	Cu(110)	$A_7 = 3.4 \times 10^{12}\ s^{-1}$, $E_7^\ddagger = 64\ kJ\ mol^{-1}$

Note. The details of the determination of these parameters are discussed in Appendix A.

5.2. *Stability of Intermediates*

Since the model is based on a statistical mechanical description of the properties of reactants and intermediates, the calculation of values of ΔH and ΔG for the reaction steps is straightforward (*15*). The reference enthalpies of formation for reaction steps 1 to 8 at 470 K, 1 atm, and $\theta = 0.5$ for each species are plotted in Fig. 1.

The reference Gibbs free energy of formation is shown in Fig. 2. The diagram shows that the reaction is nearly uphill all the way, but the net reaction is downhill. OH* plus H* is a little more stable than H_2O* due to entropy effects even though the enthalpy of

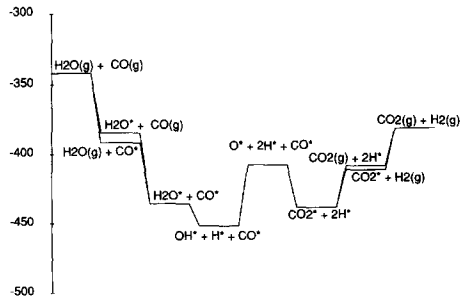

FIG. 1. Reference enthalpy of formation for the water gas shift reaction at 470 K, 1 atm, and $\theta = 0.5$.

formation of OH* plus H* is much larger than for H_2O.

The enthalpies in Fig. 1 are somewhat different from the results found by Campbell and co-workers (*4*) for reaction steps 3 and 5. These differences in the data are caused by minor differences in the kinetic models and in the computations. The differences are not significant, as both treatments with their respective data reproduce the available experiments.

5.3. *Coverages by Intermediates*

Figure 3 shows the calculated coverages by reaction intermediates on Cu(110) exposed to 10 Torr H_2O and 26 Torr CO at 543 K. The calculated coverages are small and support the approximation of vanishingly small coverages made in the determination of k_2 in Appendix A.

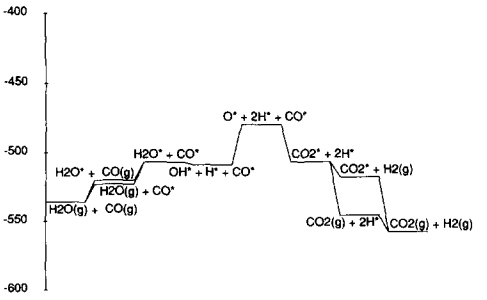

FIG. 2. Reference Gibbs free energy of formation for the water gas shift reaction at 470 K, 1 atm, and $\theta = 0.5$.

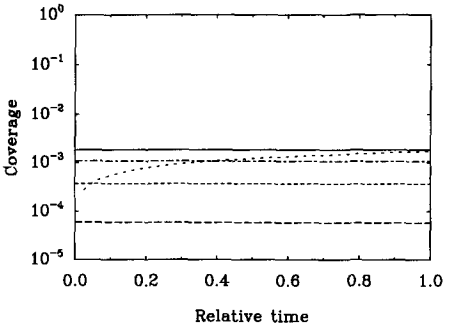

FIG. 3. Coverages of intermediates as a function of time in the batch reactor with a Cu(110) single crystal. CO* solid line, H_2O* dashed line, OH* dot dashed line, O* long dashed line, and H* dotted line. Coverages of other intermediates are very low. Initial pressures were 10 Torr of H_2O and 26 Torr of CO and temperature was 543 K. The data are directly comparable to the data presented in Fig. 8.

Figure 4 shows calculated initial coverages of OH*, H_2O*, and free sites as a function of the water content for a catalyst bed operating at 470 K and 1 atm. For large content of CO in the gas phase, water is the most abundant species on the surface, but as the H_2O/CO ratio increases hydroxide and oxygen are built up on the surface, indicating that the oxidation of CO becomes slow.

Figure 5 illustrates the coverages through a catalyst bed where we let the reaction pro-

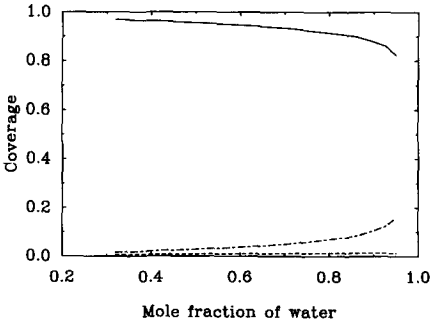

FIG. 4. Calculated initial coverages vs mole fraction of water for a catalyst bed operating at 470 K and 1 atm. * is solid, H_2O* is long dashed and OH* is dash dotted. The coverage by other intermediates is small. Input parameters are taken from Cu(111).

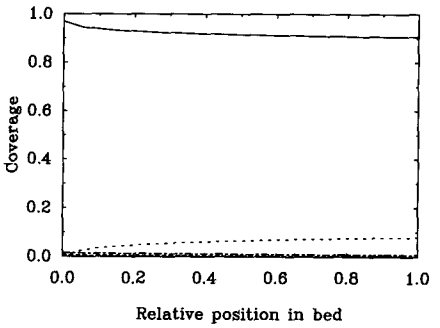

FIG. 5. Calculated coverages through a catalyst bed operating at 470 K and 1 atm. The gas composition at inlet is $x_{CO} = 0.32$, $x_{H_2O} = 0.32$, and $x_{N_2} = 0.36$ and has reached equilibrium at outlet. As CO is consumed, the coverage by H* increases. * solid line, H* dotted line, OH* dot dashed line, and H_2O* long dashed line. The coverage by other intermediates is small. Input parameters are taken from Cu(111).

ceed to equilibrium for a gas composition of $x_{CO} = 0.32$, $x_{H_2O} = 0.32$, and $x_{N_2} = 0.36$ at inlet to the catalyst bed and a temperature of 470 K and a pressure of 1 atm. At the inlet OH* is the most abundant species, but as the reaction approaches equilibrium the coverage of hydrogen increases and hydrogen the most abundant species.

We find that the increase in surface concentration of H* and the resulting decrease in the number of free sites are reflected in the calculated reaction rates, activation enthalpy, and reaction orders near equilibrium. The effect is more pronounced at high pressures. The decrease in the number of free sites near equilibrium follows from the model for a very wide range of input parameters.

Using recently determined data for the stability of formate (*17*) we find that the coverage by formate under the conditions discussed here is low. However, under high-pressure operations and in particular for gas mixtures rich in CO_2 and H_2, we predict that the coverage by formate may be substantial.

5.4. *Activation Enthalpy*

The activation enthalpy can be calculated as

$$H^{\ddagger} = k_B T^2 \left(\frac{d \ln(r_+)}{dT} \right)_p, \qquad (45)$$

where r_+ is the forward reaction rate. The form of Eqs. (26) and (27) does not immediately give us expressions for the forward or backward rate; $r = r_+ - r_-$. However, the net rate of the shift reaction can be written as (*18*)

$$r = r_+(1 - \beta), \qquad (46)$$

where

$$\beta = \frac{1}{K_g} \frac{P_{CO_2} p_{H_2}}{p_{H_2O} p_{CO}}. \qquad (47)$$

The forward rate can thus be calculated from the net rate provided the distance to equilibrium is known. The computation of $H^{\ddagger}$ from Eq. (45) is straightforward but tedious; see Appendix B. The resulting expression is too large to be shown here. A detailed investigation of that expression shows that $H^{\ddagger}$ for the shift reaction can be interpreted as the activation energy for the rate limiting step plus the averaged enthalpies of chemisorption for the intermediates. However, as steps 2, 4, and 7 may be slow, the desorption of OH* and O* may have to take place through the slow steps. The fraction that goes through each of the reactions step 2, step 4, and step 7 will be determined by the *relative* rates of these three steps. The activation enthalpy contains terms describing this change in activation enthalpy with the *relative* rates of steps 2, 4, and 7.

As an example we have calculated the overall activation enthalpy as well as the contributions to the activation enthalpy. Figure 6 shows activation enthalpy vs mole fraction of water for a catalyst bed operating at 470 K and 1 atm. At these conditions we find that increasing the coverage by adsorbed water and adsorbed hydroxide results in an increase of the overall activation enthalpy while increasing the coverage by adsorbed oxygen results in a decrease in the overall activation enthalpy. As the H_2O/CO

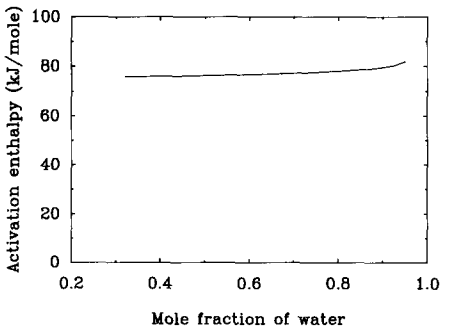

FIG. 6. Activation enthalpy vs mole fraction of water for a catalyst bed operating at 470 K and 1 atm. Adsorbed water and hydroxide result in an increase in the overall activation enthalpy while adsorbed oxygen results in a decrease in the overall activation enthalpy. As CO oxidation becomes slow, hydroxides are built up on the surface and an increase in the overall activation energy is observed. The overall activation energy decreases with increasing temperature because the coverages of intermediates decrease with increasing temperature. Input parameters are taken from Cu(111).

ratio is increased oxygen and hydroxide are built up on the surface and an increase in the overall activation energy is observed.

5.5. *Reaction Orders*

The reaction orders for the gas phase species are defined by

$$r = k_2 \left(\frac{p_{CO}}{p_0}\right)^{\alpha_{CO}} \left(\frac{p_{H_2O}}{p_0}\right)^{\alpha_{H_2O}} \left(\frac{p_{CO_2}}{p_0}\right)^{\alpha_{CO_2}} \left(\frac{p_{H_2}}{p_0}\right)^{\alpha_{H_2}} - \frac{k_2}{K_g} \left(\frac{p_{CO}}{p_0}\right)^{1+\alpha_{CO}} \left(\frac{p_{H_2O}}{p_0}\right)^{1+\alpha_{H_2O}} \times \left(\frac{p_{CO_2}}{p_0}\right)^{-1+\alpha_{CO_2}} \left(\frac{p_{H_2}}{p_0}\right)^{-1+\alpha_{H_2}} \quad (48)$$

and can be calculated as

$$\alpha_i = \left(\frac{\partial \ln(r_+)}{\partial \ln(p_i/p_0)}\right). \quad (49)$$

Again the calculation is straightforward but tedious; see Appendix B. A detailed analysis shows that the reaction orders have a simple relation to the coverages by intermediates. Again we find terms describing the *relative* rates of steps 2, 4, and 7 in the general expression.

As an example we have calculated the reaction orders for a catalyst bed operating at 470 K and 1 atm for different water contents, Fig. 7. For low water content the reaction order of water is unity, where as the reaction order for CO is zero. As the concentration of water is increased hydroxide builds up on the surface, the reaction orders change, and the reaction order of water changes from unity to zero, whereas the reaction order of CO changes from zero to unity.

5.6. *Reaction Step 7 in Equilibrium*

The rate of reaction step 7 is of no consequence for the rate of the overall reaction when reaction step 7 makes several turnovers *in both directions* for each net turnover of the overall reaction. Reaction step 7 is thus able to keep up with the overall reaction. From calculations based on the full model with the estimated parameters, Section 6, we find that the case with reaction step 2 rate limiting and reaction step 4 not running, since reaction step 3 is dominating OH* conversion, is the relevant case for the forward shift reaction.

For a catalyst operating under steady state, we *always* have $r = \frac{1}{2}(r_2 + r_4) = r_7$. The statement that reaction step 2 is rate-limiting cannot be interpreted as $r = \frac{1}{2}r_2$,

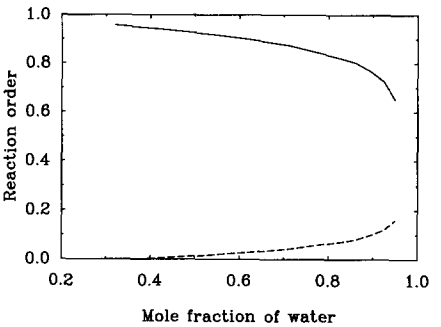

FIG. 7. Calculated reaction order vs mole fraction of water for a catalyst operating at 470 K and 1 atm. Reaction order of water, solid line, reaction order of CO, dashed line. As hydroxide is built up on the surface the reaction order of water changes from unity to zero whereas the reaction order of CO changes from zero to unity. Input parameters are taken from Cu(111).

since this equation only tells something about the stoichiometry of the net reaction. In the case where reaction 2 is rate-limiting, the equation $r = \frac{1}{2}(r_2 + r_4) = r_7$ is replaced by $r = \frac{1}{2}r_2$ *and* the equilibrium equation for step 7.

The condition under which reaction step 7 can be considered in equilibrium can be investigated from the equation determining the coverage of O*,

$$a\theta_{O*} + b\theta_{O*}^{1/2}\theta_*^{1/2} - c\theta_* = 0, \qquad (50)$$

where a, b, and c are defined by Eqs. (23)–(25). Equation (50) is an equation of the second order in $\theta_{O*}^{1/2}$. The case of reaction step 7 in equilibrium can be found from the limit $k_7 \to \infty$. In this case Eq. (50) reduces to

$$K_6K_7K_8\frac{p_{CO}}{p_0}\theta_{O*} = \frac{p_{CO_2}}{p_0}\theta_*. \qquad (51)$$

This is exactly the solution one would obtain by substituting $k_4 = 0$ and the equilibrium equation for step 7 into Eqs. (2)–(8) and (13)–(15). The equations for the coverages are reduced to

$$\theta_{H_2O*} = K_1\frac{p_{H_2O}}{p_0}\theta_* \qquad (52)$$

$$\theta_{OH*} = \left(\frac{K_1}{K_3K_6K_7K_8}\frac{p_{CO_2}p_{H_2O}}{p_{CO}\,p_0}\right)^{1/2}\theta_* \qquad (53)$$

$$\theta_{H*} = \left(\frac{1}{K_5}\frac{p_{H_2}}{p_0}\right)^{1/2}\theta_* \qquad (54)$$

$$\theta_{CO*} = K_6\frac{p_{CO}}{p_0}\theta_* \qquad (55)$$

$$\theta_{O*} = \frac{1}{K_6K_7K_8}\frac{p_{CO_2}}{p_{CO}}\theta_* \qquad (56)$$

$$\theta_{CO_2*} = \frac{1}{K_8}\frac{p_{CO_2}}{p_0}\theta_* \qquad (57)$$

$$\theta_*^{-1} = 1 + K_1\frac{p_{H_2O}}{p_0} + \left(\frac{K_1}{K_3K_6K_7K_8}\frac{p_{CO_2}p_{H_2O}}{p_{CO}\,p_0}\right)^{1/2} + \left(\frac{1}{K_5}\frac{p_{H_2}}{p_0}\right)^{1/2} + K_6\frac{p_{CO}}{p_0} + \frac{1}{K_6K_7K_8}\frac{p_{CO_2}}{p_{CO}} + \frac{1}{K_8}\frac{p_{CO_2}}{p_0} \qquad (58)$$

and the rate becomes

$$r = \frac{1}{2}k_2K_1\left(\frac{p_{H_2O}}{p_0} - \left(\frac{1}{K_g}\frac{p_{CO_2}p_{H_2O}p_{H_2}}{p_{CO}p_0^2}\right)^{1/2}\right)\theta_*^2. \qquad (59)$$

In this case the net rate of the reaction can be split in a unique way into a difference between a forward rate r_+ and a backward rate r_-,

$$r = r_+ - r_- \qquad (60)$$

$$r_+ = \frac{1}{2}k_2K_1\frac{p_{H_2O}}{p_0}\theta_*^2 \qquad (61)$$

$$r_- = \frac{1}{2}\frac{k_2K_1}{K_g^{1/2}}\left(\frac{p_{CO_2}p_{H_2O}p_{H_2}}{p_{CO}p_0^2}\right)^{1/2}\theta_*^2. \qquad (62)$$

When water dissociation is rate-limiting, the expression for the activation enthalpy is reduced to

$$H^\ddagger = H_2^\ddagger + H_1 - 2H_1\theta_{H_2O*} - 2H_6\theta_{CO*} + 2H_8\theta_{CO_2*} + 2(H_6 + H_7 + H_8)\theta_{O*} + H_5\theta_{H*} - (H_1 - H_3 - H_6 - H_7 - H_8)\theta_{OH*}. \qquad (63)$$

At this point we are able to interpret Eq. (63) in detail as in Table 4.

In Eq. (63) $H^\ddagger$ is a sum of the activation enthalpy for the rate-limiting step and a weighted average of the desorption enthalpies for the intermediates. The average is formed by multiplying the coverage for each intermediate by twice the enthalpy of desorption for the intermediate through equilibrium steps. The factor of two enters as the rate-limiting step requires two free sites. We may thus interpret $H^\ddagger$ as the sum of the activation enthalpy for the rate-limiting step plus the averaged cost of creating two free

TABLE 4

Interpretation of Desorption Enthalpies from Eq. (63)

Coefficient	Enthalpy	Reaction
1	$H_1 + H_2^{\ddagger}$	$H_2O(g) + 2* \rightleftharpoons OH* + H*$
θ_{CO*}	$-2H_6$	$2CO* \rightleftharpoons 2CO + 2*$
θ_{CO_2*}	$2H_8$	$2CO_2* \rightleftharpoons 2CO_2 + 2*$
θ_{H_2O*}	$-2H_1$	$2H_2O* \rightleftharpoons 2H_2O + 2*$
θ_{OH*}	$-H_1 + H_3 + H_6 + H_7 + H_8$	$2OH* + CO(g) \rightleftharpoons H_2O(g) + CO_2(g) + 2*$
θ_{H*}	H_5	$2H* \rightleftharpoons H_2 + 2*$
θ_{O*}	$2(H_6 + H_7 + H_8)$	$2CO(g) + 2O* \rightleftharpoons 2CO_2(g) + 2*$

sites on the surface. Actually this form of the activation enthalpy is found in general and not just in special cases. As the coverages depend on the reaction conditions we predict that the activation enthalpy should depend on the reaction conditions.

When water dissociation is rate-limiting the reaction orders have a simple relation to the coverages,

$$\alpha_{H_2O} = 1 - 2\theta_{H_2O*} - \theta_{OH*} \tag{64}$$

$$\alpha_{CO} = 2\theta_{O*} + \theta_{OH*} - 2\theta_{CO*} \tag{65}$$

$$\alpha_{CO_2} = -2\theta_{CO_2*} - 2\theta_{O*} - \theta_{OH*} \tag{66}$$

$$\alpha_{H_2} = -\theta_{H*} \tag{67}$$

As the reaction orders depend on the coverages, we predict that the reaction orders should depend on the reaction conditions.

5.7. *Reactions Step 2 and Step 4 in Equilibrium*

In the case where reaction step 2 and/or step 4 makes several turnovers for each turnover of the net reaction, reaction steps 2 and 4 are able to keep up with the overall reaction and the rate of the net reaction will be determined by reaction step 7. In this limit we have $r_+ = r_{+7}$ and $r_- = r_{-7}$. When reaction step 7 is rate-limiting, the equations for steps 2 and 3 or steps 3 and 4 convey the same information since the formation of OH* is in equilibrium. Inspection of Eq. (50) gives for $k_3 \to \infty$

$$\left(\frac{P_{H_2}}{p_{H_2O}}\right)\theta_{O*} = K_1K_2^2K_3K_5\theta_*. \tag{68}$$

The coverages of intermediates are

$$\theta_{H_2O*} = K_1\frac{p_{H_2O}}{p_0}\theta_* \tag{69}$$

$$\theta_{OH*} = K_1K_2K_5^{1/2}\frac{p_{H_2O}}{p_0^{1/2}p_{H_2}^{1/2}}\theta_* \tag{70}$$

$$\theta_{H*} = \left(\frac{1}{K_5}\frac{p_{H_2}}{p_0}\right)^{1/2}\theta_* \tag{71}$$

$$\theta_{CO*} = K_6\frac{p_{CO}}{p_0}\theta_* \tag{72}$$

$$\theta_{O*} = K_1K_2^2K_3K_5\frac{p_{H_2O}}{p_{H_2}}\theta_* \tag{73}$$

$$\theta_{CO_2*} = \frac{1}{K_8}\frac{p_{CO_2}}{p_0}\theta_* \tag{74}$$

$$\theta_*^{-1} = 1 + K_1\frac{p_{H_2O}}{p_0} + K_1K_2K_5^{1/2}\frac{p_{H_2O}}{p_0^{1/2}p_{H_2}^{1/2}} + \left(\frac{1}{K_5}\frac{p_{H_2}}{p_0}\right)^{1/2} + K_6\frac{p_{CO}}{p_0} + K_1K_2^2K_3K_5\frac{p_{H_2O}}{p_{H_2}} + \frac{1}{K_8}\frac{p_{CO_2}}{p_0} \tag{75}$$

and the rate is

$$r = \frac{k_7}{K_7K_8}\left(K_g\frac{p_{H_2O}p_{CO}}{p_{H_2}p_0} - \frac{p_{CO_2}}{p_0}\right)\theta_*^2. \tag{76}$$

When reaction step 7 is rate-limiting, the general expression for the activation enthalpy for the overall reaction is reduced to

$$H^{\ddagger} = H_7^{\ddagger} + H_1 + 2H_2 + H_3 + H_5 + H_6 - 2H_1\theta_{H_2O*} - 2H_6\theta_{CO*} + 2H_8\theta_{CO_2} - 2(H_1 + 2H_2 + H_3 + H_5)\theta_{O*} + H_5\theta_{H*} - 2(H_1 + H_2 + \tfrac{1}{2}H_5)\theta_{OH*}. \tag{77}$$

Again this can be interpreted as a sum of the activation enthalpy for the rate limiting step

TABLE 5

Interpretation of Desorption Enthalpies from Eq. (77)

Coefficient	Enthalpy	Reaction
1	$H_7^{\ddagger} + H_1 + 2H_2 + H_3 + H_5 + H_6$	$H_2O(g) + CO(g) + * \rightleftharpoons H_2(g) + CO_2*$
θ_{CO*}	$-2H_6$	$2CO* \rightleftharpoons 2CO + 2*$
θ_{CO_2*}	$2H_8$	$2CO_2* \rightleftharpoons 2CO_2 + 2*$
θ_{H_2O*}	$-2H_1$	$2H_2O* \rightleftharpoons 2H_2O + 2*$
θ_{OH*}	$-2(H_1 + H_2 + \frac{1}{2}H_5)$	$H_2(g) + 2OH* \rightleftharpoons 2H_2O(g) + 2*$
θ_{H*}	H_5	$2H* \rightleftharpoons H_2 + 2*$
θ_{O*}	$-2(H_1 + 2H_2 + H_3 + H_5)$	$2H_2(g) + 2O* \rightleftharpoons 2H_2O(g) + 2*$

and a weighted average of the desorption enthalpies for the intermediates; see Table 5.

When CO oxidation is rate-limiting the reaction orders are given by

$$\alpha_{H_2O} = 1 - 2(\theta_{H_2O*} + \theta_{OH*} + \theta_{O*}) \quad (78)$$

$$\alpha_{CO} = 1 - 2\theta_{CO*} \quad (79)$$

$$\alpha_{CO_2} = -2\theta_{CO_2} \quad (80)$$

$$\alpha_{H_2} = -1 + \theta_{OH*} - \theta_{H*} + 2\theta_{O*}. \quad (81)$$

6. REACTION CALCULATIONS

As mentioned in the introduction we are investigating the redox mechanism by treating each of the reaction steps as well as the catalytic reaction using one model to see if a coherent and reasonably accurate description is obtained. The use of a single model is of major importance for the discussion of the agreement between calculation and experiment for the catalytic reaction, as we cannot adjust the parameters in the model to improve the agreement with one experiment without reexamining the consequences for other aspects of the model. The agreement with experiments for the catalytic reaction rate could of course be improved somewhat if we did not require that the model should give a reasonable treatment of the kinetics and thermodynamics of each of the reaction steps.

The two asymptotic solutions studied in the previous section are useful as reference points in the study of the full model. The computation of the coverages show that these will be low and can be neglected in rough estimates of the kinetics we expect to see. When the water concentration is low, water dissociation must become rate-limiting, and the activation energy and reaction orders must be close to the values given by Eqs. 63–67. Under these conditions the reaction is first order in H_2O and zeroth order in CO and the dominating contribution to the activation enthalpy is the activation enthalpy for the partial reaction made up of steps 1 and 2. As the H_2O/CO ratio decreases, the oxidation of CO, step 7, must eventually become rate-limiting. We thus expect to see a transition toward a situation where the reaction is first order in H_2O and CO and negative for H_2. The activation enthalpy for the catalytic reaction will equal the activation enthalpy for the partial reaction made up of steps 1, 2, 3, 4, 5, 6, and 7.

Very few studies of the WGS reaction on a working Cu-based catalyst have been published. Among the few publications (*7–9, 12*) on the WGS reaction on Cu-based catalysts, only Herwijnen *et al.* (*8, 9*) have published a full data set suitable for testing a kinetic model as presented here. Herwijnen and de Jong (*8*) and Herwijnen (*9*) report the initial rate in a mixture of CO, H_2O, and N_2; this simplifies our calculations as no integration is necessary to determine this rate. However, for the investigation of the kinetics at higher conversions as well as for the calculation for the single crystal batch reactor, an integration of the rate equation is necessary. We do this by first calculating the partition functions, using the data listed in Table 2. From this we calculate the equilibrium constants, Eqs. (37)–(44). The rate constants are calculated from the data in Table 3 and Eqs. (37)–(44). We then perform an integration using an adaptive stepsize Runge–Kutta routine (*19*); the rate at each step is calculated from the gas phase composition using Eq. (26). The most unconven-

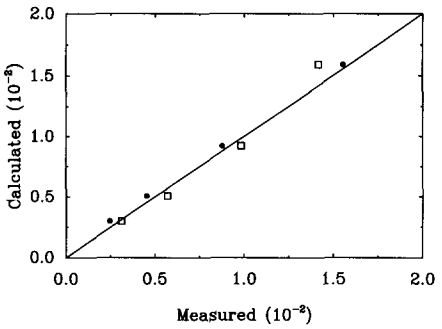

FIG. 8. Calculated exit mole fraction of hydrogen (solid circles) and carbon dioxide (open squares) versus measured exit mole fraction for Cu(110). The initial gas phase composition is 10 Torr H_2O and 26 Torr CO and the temperatures are 543, 573, 612, and 653 K. The coverage by intermediates is negligible in this experiment, Appendix A and Fig. 3.

tional aspect of the program is the size of the rate expression.

In the calculations we treat the gas phase as ideal, we neglect diffusion limitations and heat transfer phenomena, and we treat the reactor as isothermal and the flow pattern as ideal back-mix or ideal plug-flow. However, the reaction is structure sensitive, Tables 2 and 3 and Appendix A, and it is important to use the parameters for the relevant surface.

We start the comparison between calculation and experiment by noting that the calculated value for the gas phase equilibrium constant is within a few percent of the accepted value (*1*).

The kinetic data for reaction 2, Table 3 were deduced from the single crystal experiment under the assumption of negligible coverage by intermediates. Figure 8 shows a comparison of the experimental and calculated exit mole fractions of H_2 and CO_2 for the Cu(110) experiment. The agreement between model and experiment is satisfactory. This as well as the calculation of the coverages, Section 5.3, shows that the assumption of negligible coverage under these conditions is valid.

Initial rates measured by Herwijnen and de Jong (*8*) and Herwijnen (*9*) for the forward shift reaction were measured using a commercial (Cu,Zn,Fe)-catalyst. The inlet gas consisted of CO, H_2O and N_2. N_2 is an inert. The experiments were performed in a plug flow reactor in the limit of low conversion at 445–501 K and 1 atm total pressure. Both the dissociation of water and the oxidation of CO may be rate-limiting under these conditions as the reaction mixture is varied essentially from a H_2O + N_2-mixture to a CO + N_2 mixture. The rate at these conditions is

$$r = \frac{1}{2} k_2 K_1 \frac{p_{H_2O}}{p_0} \theta_*^2 \tag{82}$$

and surface coverages are

$$\theta_{H_2O*} = K_1 \frac{p_{H_2O}}{p_0} \theta_* \tag{83}$$

$$\theta_{OH*} = \left(\frac{K_1}{K_3} \frac{p_{H_2O}}{p_0} \frac{1}{2} \frac{k_2 K_1}{k_7 K_6} \frac{p_{H_2O}}{p_{CO}} \right)^{1/2} \theta_* \tag{84}$$

$$\theta_{H*} = 0 \tag{85}$$

$$\theta_{CO*} = K_6 \frac{p_{CO}}{p_0} \theta_* \tag{86}$$

$$\theta_{O*} = \frac{1}{2} \frac{k_2 K_1}{k_7 K_6} \frac{p_{H_2O}}{p_{CO}} \theta_* \tag{87}$$

$$\theta_{CO_2*} = 0 \tag{88}$$

$$\theta_*^{-1} = 1 + K_1 \frac{p_{H_2O}}{p_0} + \left(\frac{K_1}{K_3} \frac{p_{H_2O}}{p_0} \right)^{1/2} \left(\frac{1}{2} \frac{k_2 K_1}{k_7 K_6} \frac{p_{H_2O}}{p_{CO}} \right)^{1/2} + K_6 \frac{p_{CO}}{p_0} + \frac{1}{2} \frac{k_2 K_1}{k_7 K_6} \frac{p_{H_2O}}{p_{CO}}. \tag{89}$$

Since the reaction is structure sensitive we investigate the agreement between calculation and experiment using the parameters for Cu(111) as well as for Cu(110).

Figure 9 shows calculated and experimental initial rates for the shift reaction versus the mole fraction of water in the gas phase. Model parameters are taken from Cu(111). The rate constants used in the model calculations are those listed in Table 3 and the

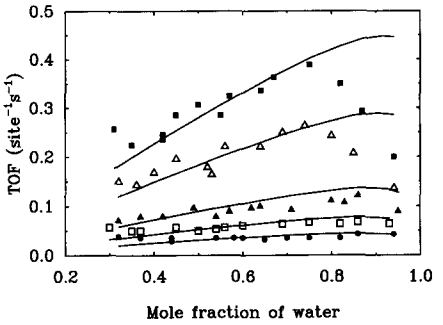

FIG. 9. Calculated initial rates (solid curve) and measured initial rates (symbols) for the forward shift reaction versus mole fraction of water. The temperatures for the five series are 445 K (solid circle), 457 K (open square), 470 K (solid triangle), 489 K (open triangle), and 501 K (solid square). The gas contains N_2 in the ratio $CO/N_2 = 0.89$. Input parameters are taken from Cu(111).

rate expression is Eq. 26. The number of active sites in the catalyst has not been reported and must be determined by fitting the reaction data. This is the only free parameter in the model. The estimated active surface area is 5×10^{-5} mol sites/g catalyst which is 3.4 m^2/g catalyst. This area is 15% of the measured BET area before reduction, which is not unreasonable.

The calculated initial rates are in reasonable agreement with measured initial rates over the ranges of temperature and composition spanned by the experimental data set. However, for high water contents and high temperatures, 489 and 501 K, we calculate a rate which is systematically higher than the experimental value. To quantize the agreement between experiment and calculation, we have calculated the correlation coefficient r between calculation and experiment. For Cu(111) we find $r = 0.93$. If we neglect the four outlier points at high temperature and high water content, we find $r = 0.98$. This illustrates that the agreement between experiment and calculation is actually quite good and the model deviates from experimental observation only at a few points.

Calculation of surface coverages of H_2O* and OH* as a function of the water content in the inlet gas, Section 5.3, shows that the coverage of water and carbon monoxide is very low for all gas compositions, whereas the coverage of hydroxide and oxygen increases as the p_{H_2O}/p_{CO} ratio increases. However, the coverage of oxygen is still very low. At low partial pressures of H_2O, the dissociation of H_2O, reaction step 2, is rate-limiting. At high partial pressures of H_2O reaction step 2 is still the slowest; however, the build up of hydroxide indicates that the oxidation of CO step 7 has become slow, as a consequence of the low content of CO in the gas.

Figure 10 shows the result of the same calculation as in Fig. 9, except that the parameters for the calculation have now been taken for the Cu(110) surface. Here we observe that for low water content theory and experiment are in agreement but for high water content the model again predicts a higher rate than experiment. The turnover frequency is about 10 times higher for Cu(110) than for Cu(111), reflecting the structure sensitivity of this reaction. If the active area consists of Cu(110) the active area of the catalyst is ~2% of the BET area

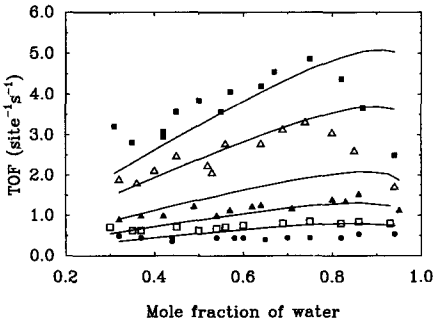

FIG. 10. Calculated initial rates (solid curve) and measured initial rates (symbols) for the forward shift reaction versus mole fraction of water. The temperatures for the five series are 445 K (solid circle), 457 K (open square), 470 K (solid triangle), 498 K (open triangle), and 501 K (solid square). The gas contains N_2 in the ratio $CO/N_2 = 0.89$. Input parameters are determined from Cu(110) and the number of active sites for the catalyst is scaled to optimal agreement between calculation and experiment.

of the catalyst. The correlation coefficient is $r = 0.92$, and if we again neglect the four outlier points we find $r = 0.97$, illustrating a good agreement between model and experiment at most of the experimental conditions.

From the high turnover frequency of Cu(110) it can be concluded that if Cu(110) constitute a significant fraction of the active area, only an unreasonably low fraction, <2%, of the total area is active. The catalyst used in the experiments (*9*) consists of small Cu particles dispersed on ZnO and Fe_2O_3. Simulation of small clusters of Cu at high temperatures show that the surface of the clusters consists mainly of close-packed surfaces (*20*). This observation supports the view that the active area of the catalyst effectively consist of Cu(111) planes. Therefore the description of the catalyst as effectively consisting of Cu(111) surfaces seems to be a reasonable assumption.

7. ANALYSIS OF THE PARAMETERS

Two interesting questions are how many of the vast number of parameters have any importance for the calculated rate under the conditions considered here and whether we know these parameters sufficiently accurately to calculate the rate reliably. For the experimental data considered here the results of our calculations are only significantly sensitive to the values of k_2 and k_7 and the binding energies of H_2O*, CO*, OH*, and O*. The results are independent of the binding energies of H* and CO_2*, since the coverage of these intermediates is zero at the conditions of the experimental data in Figs. 7 and 8. For this reason the sensitivity analysis may not be complete if other conditions are considered.

Calculations using the sticking coefficients for H_2O, H_2, CO, and CO_2 show that steps 1, 5, 6, and 8 cannot be rate-limiting under the conditions considered here. The model is thus internally consistent with respect to the assumption of equilibrium for each for these reaction steps.

Changing the stability of H_2O*, OH*, or O* will of course change the shape of the calculated rate in Figs. 9 and 10. However, the agreement between model and experiment cannot be improved significantly without sacrificing the agreement between model and experiment for TPD of H_2O*, TPD of OH*, the dissociative sticking coefficient for H_2O and for CO_2, or the reaction probability for the CO oxidation.

The LEED studies of OH* suggest that there is an attractive interaction between OH* species. It is not unlikely that such an interaction could be strong enough to be significant at high coverages. However, the coverages for OH* we calculate under reaction conditions are of the same magnitude as the initial coverage for the TPD experiments (*32*). For this reason, the introduction of an attractive adsorbate–adsorbate interaction for OH* cannot significantly improve the agreement between model and experiment for the catalytic reaction, Figs. 9 and 10, without significantly compromising the agreement between model and experiment for the TPD of OH*.

Calculations (*17*) shows that the coverage by formate is low under the conditions studied here even if significant amounts of formate may exist on the surface of a catalyst operating under high partial pressures of CO_2 and H_2.

As a possible explanation within the redox mechanism for the problem at high temperature and high water concentration, we note that the observed kinetics is sensitive to the value of the rate constant, k_7, for the CO oxidation. The observed decrease in the rate at high partial pressures of water and high temperatures can be described by the model if the CO oxidation rate is approximately 20 times lower than assumed in Section 6. The lower CO oxidation rate leads to a higher hydroxide coverage which leads to a decrease in the rate. As mentioned in Appendix A, this reaction has a complicated kinetics and the Langmuir–Hinschelwood kinetics used here is an approximation. However, among the published experiments on CO oxidation or O_2 dissociation on cop-

per we have found no indication of a discrepancy of this magnitude.

8. CONCLUSIONS

A kinetic model for the shift reaction has been presented. The model is based on a statistical mechanical treatment of the redox mechanism of the water gas shift reaction.

In the model formulation we neglected adsorbate–adsorbate interactions. However, we fit the ground state energy to the TPD spectra at a coverage which is relevant for the reaction calculations, and the interaction energy between adsorbates will thus be adsorbed in the ground state energy.

The simplicity of the reaction sequence for the redox mechanism is deceptive. If the reaction mixture is varied from pure H_2O to pure CO, the rate-limiting step must shift from the oxidation of CO to the dissociation of H_2O. In the formulation of our model we allow for the possibility that either or both of these reactions may determine the rate of the overall reaction. The comparison between calculated and experimental results indicates that this shift in rate-limiting step does not happen under experimentally accessible conditions, although the experimentally observed decrease in rate at high water partial pressures anticipates the change in rate-limiting step.

The model has been tested against both kinetic data measured for single crystal surfaces (*4, 10*) and kinetic data for a commercial catalyst (*8*). The comparison with catalytic rate data measured for the single crystals constitute a basic check on the validity of the kinetic model.

The reaction data for the forward shift reaction for the catalyst is in agreement with data taken from single crystal studies using Cu(111) if one assumes that the active area of the catalyst is entirely Cu(111). If one assumes that more than a percent of the total area on the catalyst is Cu(110), the experimental rate for the forward shift reaction and the redox mechanism with data measured on single crystal surfaces of Cu(110) cannot be brought into reasonable agreement. These observation suggest that the catalyst mainly consists of Cu(111) unless the active area is an unreasonably low fraction of the total area (approximately 2%).

Under most reaction conditions the coverage by reaction intermediates is small. We find that the observed maximum in the initial rate of the forward shift reaction as a function of the H_2O/CO ratio at high temperatures is not immediately consistent with input data from single crystal studies. The available data for Cu(111) are not quite as accurate as we would like for a detailed study of this phenomenon. However, the data for the stability of the intermediates and for the rate of the elementary reactions rule out the hypothesis that the maximum could be due to excessive formation of formate (*8*) or to high coverages of H_2O* at high partial pressures of water.

In principle the dissociation of H_2 must become rate-limiting for the reverse shift reaction in almost pure CO_2, but we have found no evidence that hydrogen recombination can become rate-limiting for the forward shift reaction. We have not yet found any conditions where both reactions, step 2 and step 7, are so fast that their rates approach the rate of the dissociative chemisorption of H_2.

APPENDIX A. INPUT PARAMETERS

A.1. H_2

The parameters for hydrogen molecules in gas phase are (*23*) H–H vibration ω = 4405.3 cm^{-1}, rotational constant B = 60.8 cm^{-1}, symmetry number σ = 2, and ground state energy E_e = −35 kJ mol^{-1}. The ground state energy for H_2 is estimated so that the enthalpy of formation is zero at 298.15 K.

*A.2. H**

The calculated value for the frequency of the orthogonal frustrated translation for H*/Cu(111) $\omega_\perp$ = 1291 cm^{-1} (*24*) is close to the frequency measured for H*/Ni(111),

$\omega_\perp = 1121\ \text{cm}^{-1}$ (*25*). The estimated frequency for the parallel frustrated translation is $\omega_\parallel = 157\ \text{cm}^{-1}$.

The ground state energy for hydrogen atoms on Cu can be estimated from the TPD spectra. The desorption rate is

$$\frac{d\theta_{H*}}{dt} = k_5 K_5 \frac{p_{H_2}}{p_0}\theta_*^2 - k_5\theta_{H*}^2. \qquad (90)$$

The rate constant k_5 is estimated from the sticking probability $\sigma(T)$ by

$$k_5 = \frac{p_0}{K_5\sqrt{2\pi m k_B T}}\frac{\sigma(T)}{d}, \qquad (91)$$

where d is the density of sites on the surface. In the case where the pumping rate is very high, $p_{H_2} \simeq 0$, the desorption rate is given by

$$\frac{d\theta_{H*}}{dt} = -k_5\theta_{H*}^2. \qquad (92)$$

After the frequencies for the mechanical degrees of freedom have been substituted into z_{H*}, the only parameter in z_{H*} is E_e. We determine this by fitting our solution of Eq. 92 to experimental TPD data. We do this iteratively, guessing a value for E_e, using this value in an integration of Eq. (92), comparing the calculated to the experimental desorption rate, and using this comparison to improve on E_e until the agreement between calculation and experiment is maximum. The integration is made by an adaptive stepsize Runge–Kutta routine; we calculate z_{H*} and z_{H_2} from the data above and K_5 from Eq. (41).

On both Cu(100) and Cu(110) hydrogen introduces reconstruction (*26*). These reconstructions lead to unusual peak shapes and we cannot extract the ground state energy of H* using the equations above for these highly nonideal peak shapes. On Cu(111) hydrogen desorption follows an ordinary second order desorption process, and it is therefore possible to extract a desorption energy by a simple analysis. Since a sticking coefficient for hydrogen on copper for a Boltzmann distributed gas has been determined only for the Cu(110) plane, we use this in the interpretation of the TPD spectrum of hydrogen on Cu(111). The prefactor of the sticking coefficient is 1.14 and the activation energy is 60.0 kJ mol^{-1} for Cu(110) (*27*). This value is consistent with the barrier determined from molecular beam studies (*26, 28–30*). Using these data the estimated ground state energy of hydrogen is $E_e = -27.0$ kJ mol^{-1}. We note that the estimated ground state energy may be different if the sticking coefficient for Cu(111) is significantly different from Cu(110). Figure 11 shows a calculated TPD spectrum for hydrogen on Cu(111) using this value for E_e. The calculated spectrum is very similar to the experimental spectrum (*26*) for both peak positions and shapes.

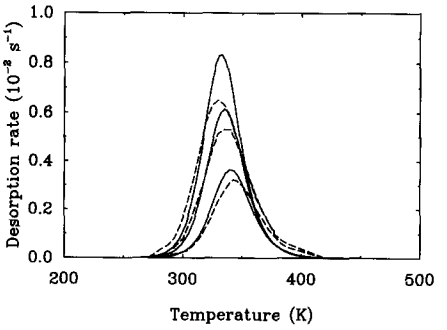

FIG. 11. Calculated (solid curve) and experimental (dashed curve) TPD spectra for H_2 on Cu(111) using initial coverages $\theta = 0.16$, $\theta = 0.26$, and $\theta = 0.35$. The more important parameters in the calculation are the ground state energy $E_e = -27.0$ kJ mol^{-1} for H* and the activation energy $E^\ddagger = 60.0$ kJ mol^{-1} for the dissociative sticking of H_2.

We estimate an adsorption energy of 27 kJ mol^{-1}, which is about 10 kJ mol^{-1} higher than the value one would get using the data quoted by Wachs and Madix (*31*) estimated for hydrogen on Cu(110). This is because the desorption temperature is higher on Cu(111) than on Cu(110) (*26*). Different models can also lead to different estimated energies (*26*). We find it important that with the estimated value we are able to reproduce the experiment.

A.3. H_2O

The parameters for water in gas phase are (*23*) scissor mode $\omega_1 = 1594.6\ cm^{-1}$, O–H stretch $\omega_2 = 3657.1\ cm^{-1}$, O–H stretch $\omega_3 = 3755.8\ cm^{-1}$, symmetry number $\sigma = 2$, product of moment of inertia $I_A I_B I_C = 5.7658 \times 10^{-141}\ kg^3m^6$, and ground state energy $E_e = -306\ kJ\ mol^{-1}$.

A.4. H_2O*

The adsorption of H_2O on Cu(110) has been studied in some detail. EELS shows that water adsorbs as hydrogen-bonded clusters of molecules at all coverages (*32, 33*). We assume that the hydrogen bonding prevents the free rotation of the adsorbed molecules.

Parameters for adsorbed water are (*33*) scissor mode $\omega_1 = 1600\ cm^{-1}$, O–H stretch $\omega_2 = 3370\ cm^{-1}$, O–H stretch $\omega_3 = 3370\ cm^{-1}$, librations $\omega_4 = 745\ cm^{-1}$, frustrated orthogonal translation $\omega_\perp = 460\ cm^{-1}$, frustrated parallel translation $\omega_\parallel = 21\ cm^{-1}$.

The adsorption energy for H_2O* is ~50 kJ mol^{-1}, clearly indicating that H_2O* is in a physisorbed state. One would thus not expect to see significant differences in ground state energy for H_2O* between different surfaces of Cu.

The TPD spectrum of adsorbed H_2O shows maximum desorption at 175 K at low coverages. The peak temperature *increases* 5–10 K with increasing coverage (*32, 33*) which indicates an attractive interaction between adsorbed water molecules. The sticking coefficient of water is unity (*33*). The rate of desorption of water is given by

$$\frac{d\theta_{H_2O*}}{dt} = -\frac{k_1}{K_1}\theta_{H_2O*}, \qquad (93)$$

where k_1 is the rate constant for water adsorption. The ground state energy of H_2O can be estimated assuming that the sticking coefficient for water adsorption is unity. The calculated ground state energy for $H_2O*/Cu(110)$ is $E_e = -365\ kJ\ mol^{-1}$.

For water on Cu(111) the TPD peak for desorption has been measured to be 150 K (*34, 35*). The monolayer peak cannot be separated from the multilayer peak. For water on Cu(111) the ground state energy is estimated to be $E_e = -359\ kJ\ mol^{-1}$, which gives an adsorption energy of ~44 kJ mol^{-1}, equal to the heat of sublimation of ice. This confirms that the difference in the heat of adsorption between the different surfaces is small.

*A.5. O**

The parameters for adsorbed atomic oxygen on Cu(110) are orthogonal frustrated translation $\omega_\perp = 391\ cm^{-1}$ and parallel frustrated translation $\omega_\parallel = 508\ cm^{-1}$ (*36*). The ground state energy of oxygen on Cu cannot be estimated from TPD experiments because oxygen penetrates into the bulk during the heating of the crystal. Since we have a description of the thermodynamics for CO* (Section A.8) and CO_2* (Section A.9) the carbon monoxide oxidation reaction step 7,

$$CO* + O* \rightleftharpoons CO_2*, \qquad (94)$$

offers a possibility of determining the ground state energy of O*. From microscopic reversibility we have

$$K_7 = \frac{k_{7+}}{k_{7-}}. \qquad (95)$$

The forward rate constant k_{7+} can be determined from the reaction probability for CO oxidation on an oxygenated surface, whereas the reverse rate constant k_{7-} can be determined from the dissociation probability of CO_2. By assuming that the forward and reverse reactions follow simple Langmuir kinetics, it is possible to estimate the ground state energy of adsorbed oxygen. The CO oxidation reaction does show complicated kinetics (*37*) and therefore it is an approximation to use simple Langmuir kinetics.

k_{7+} is given by

$$k_{7+} = \frac{1}{K_6}\frac{p_0}{(2\pi m k_B T)^{1/2}}\frac{1}{\theta_{O*}\theta_*}\bar{\sigma}_{CO}\frac{1}{d}, \qquad (96)$$

where $\bar{\sigma}_{CO}$ is the reaction probability for CO oxidation on a surface with oxygen coverage θ_{O*} and d is the density of sites. k_{7-} is given by

$$k_{7-} = K_8 \frac{p_0}{(2\pi m k_B T)^{1/2}} \frac{1}{d} \bar{\sigma}_{CO_2}, \quad (97)$$

where $\bar{\sigma}_{CO_2}$ is the dissociation probability for CO_2 on a clean surface. k_{7+} and k_{7-} inserted in Eq. (95) give

$$K_7 = \frac{1}{K_6 K_8} \left(\frac{M_{CO_2}}{M_{CO}}\right)^{1/2} \frac{\bar{\sigma}_{CO}}{\bar{\sigma}_{CO_2}} \frac{1}{\theta_{O*}\theta_*} \quad (98)$$

M_{CO} and M_{CO_2} are the molar masses of CO and CO_2. The only unknown parameter in this equation is the ground state energy of adsorbed oxygen. Campbell and co-workers have determined $\bar{\sigma}_{CO}$ (*38*) and $\bar{\sigma}_{CO_2}$ (*4*) on Cu(110),

$$\bar{\sigma}_{CO} = 4.8 \times 10^{-3} \exp\left(\frac{-27 \text{ kJ/mol}}{RT}\right) \quad (99)$$

$$\bar{\sigma}_{CO_2} = 1.1 \times 10^{-3} \exp\left(\frac{-67 \text{ kJ/mol}}{RT}\right). \quad (100)$$

From these values the ground state energy of adsorbed oxygen is determined to be $E_{O*} = -243$ kJ mol^{-1}. The estimated heat of adsorption is actually very close to the measured heat of adsorption of oxygen on polycrystalline copper (*39*).

For lack of data, we assume the same ground state energy for O* on Cu(111) as for Cu(110), $E_{O*} = -243$ kJ mol^{-1}. The validity of this assumption is discussed in Section A.6.

*A.6. OH**

Vibrational frequencies for hydroxide adsorbed on Ag(110) have been published (*40*) and these vibrational frequencies are used as an estimate of the vibrational frequencies of OH/Cu(110): orthogonal frustrated translation $\omega_\perp = 280$ cm^{-1}, parallel frustrated translation $\omega_\parallel = 670$ cm^{-1}, and O–H stretch $\omega = 3380$ cm^{-1}.

The ground state energy of hydroxide on Cu can be estimated from TPD experiments. The net reaction for the desorption is

$$2OH* \rightleftharpoons H_2O(g) + O* + *. \quad (101)$$

In the model outlined by the reactions step 1–step 8 there are two possible paths for the disproportionation of OH*. One possibility is

$$OH* + * \rightleftharpoons O* + H* \quad (102)$$

$$OH* + H* \rightleftharpoons H_2O* + * \quad (103)$$

$$H_2O* \rightleftharpoons H_2O(g) + * \quad (104)$$

with reaction 103 rate limiting. The other possibility is the direct disproportionation

$$2OH* \rightleftharpoons H_2O(g) + O* + *. \quad (105)$$

In the case of infinite pumping rate $p_{H_2O} \sim 0$ the former mechanism gives the desorption rate

$$\frac{d\theta_{OH*}}{dt} = -\frac{k_2}{K_2} \theta_{OH*}\theta_{H*}, \quad (106)$$

where

$$\theta_{H*} = K_4 \frac{\theta_{OH*}\theta_*}{\theta_{O*}} \quad (107)$$

$$\theta_{O*} = \frac{1}{2}(\theta^i_{OH*} - \theta_{OH*}) \quad (108)$$

$$\theta_* = \frac{1}{2} \frac{(1 - (1/2)(\theta^i_{OH*} + \theta_{OH*}))(\theta^i_{OH*} - \theta_{OH*})}{\theta_{OH*}(K_4 - 1/2) + (1/2)\theta^i_{OH*}}. \quad (109)$$

θ^i_{OH*} is the initial coverage of OH*. The other mechanism gives the rate

$$\frac{d\theta_{OH*}}{dt} = k_3 \theta^2_{OH*}. \quad (110)$$

k_3 can be calculated from the reaction probability of water on an oxygen covered surface. The dissociative reaction probability of water on a surface with an oxygen coverage of 0.12 is near unity at 100 K (*4, 32, 41*).

By considering both desorption paths in the calculation we find that removal of OH*

through Eq. (105) is much faster than removal through Eqs. (102)–(104).

The temperature of maximum desorption of hydroxide on Cu(110) is 290 K (*32*). Using this temperature with the thermodynamic data for H_2O* and $O*$ (Sections 4.4 and 4.5) and the vibration frequencies listed above we find $E_e = -329$ kJ mol^{-1}. We estimate the enthalpy for the reaction to be 99 kJ mol^{-1}. This value is somewhat higher than the value estimated by Campbell and coworkers (*4*). While calculated spectra and the calculated value for k_3 near the peak maximum are very similar, differences in the calculational procedures gives somewhat different values when k_3 is resolved into an activation energy and a preexponential factor.

For lack of data, we assume the same ground state energy for OH* on Cu(111) as for Cu(110), $E_e = -319$ kJ mol^{-1}. At this state we should point out that in the following calculations, it is only the difference in ground state energy between O* and OH* that is important. The individual values of the ground state energies of O* and OH* are not important. The binding energy of oxygen does vary for the different surface planes (*42*) and so does the binding energy of hydroxide, but the difference in binding energy will probably not vary significantly for the different surface planes. Therefore we consider it a good approximation to use the same binding energy for O* and OH* for the Cu(110) and Cu(111) plane.

Figure 12 shows a calculated TPD spectrum for OH/Cu(110).

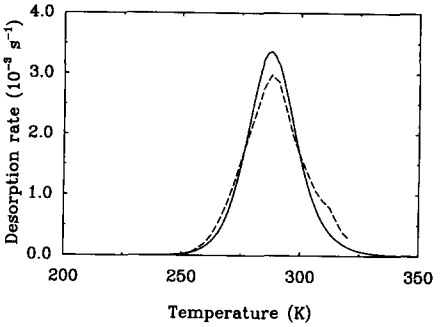

FIG. 12. Calculated (solid curve) and experimental (dashed curve) (*32*) TPD spectra for hydroxide disproportionation on Cu(110). The initial coverage is 0.09.

A.7. CO

Parameters for carbon monoxide in gas phase are (*23*) C–O vibration $\omega = 2169.5$ cm^{-1}, rotational constant B = 1.9 cm^{-1}, symmetry number $\sigma = 1$, and ground state energy $E_e = -130$ kJ mol^{-1}. The ground state energy for CO is estimated so that the enthalpy of formation is -110.59 kJ mol^{-1} at 298.15 K.

*A.8. CO**

The measured frequencies for CO stretch on Cu(111), Cu(110), and Cu(100) are very similar: $\omega = 2077$ cm^{-1} on Cu(111) (*43*), $\omega = 2088$ cm^{-1} on Cu(110) (*21*), and $\omega = 2089$ cm^{-1} on Cu(100) (*44*). Frustrated orthogonal translation $\omega_\perp = 342$ cm^{-1} on Cu(100) (*44*) and $\omega_\perp = 330$ cm^{-1} on Cu(111) (*43*). We estimate that the frustrated parallel translation $\omega_\parallel = 17$–170 cm^{-1}. The choice of $\omega_\parallel$ in this range has no significant influence for the interpretation of the TPD spectrum.

The sticking coefficient for CO on Cu(110) is 0.5 (*22*). The ground state energy for CO on Cu(110) is estimated from TPD experiments. The ground state energy is $E_e = -190$ kJ mol^{-1}. The calculated spectrum is in reasonable agreement with the experimental spectra (*21, 22*).

The ground state energy of CO on Cu(100) estimated from TPD measurements (*45*) is $E_e = -181$ kJ mol^{-1}. This value is used for CO/Cu(111).

A.9. CO_2

The parameters for CO_2 are (*23*) $\omega_1 = 1342.9$ cm^{-1}, $\omega_2 = 667.3$ cm^{-1} degenerated, $\omega_3 = 2349.3$ cm^{-1}, rotational constant B = 0.39 cm^{-1}, symmetry number $\sigma = 2$, ground state energy $E_e = -431$ kJ mol^{-1}.

*A.10. CO_2**

CO_2 is physisorbed on Cu (*46, 47*). CO_2 is physisorbed through its oxygen atoms but is almost linearly bound to the surface. Therefore it is assumed that the vibrational

spectrum for CO_2* consist of the vibrational modes found in the free molecule in addition to the frustrated translation. For CO_2/Ni(110) the frequencies have been measured and are almost identical to the gas phase vibrational frequencies.

For CO_2/Cu(110) we use the measured frequencies for CO_2/Ni(110) (*48*), $\omega_1 = 1343\ cm^{-1}$, $\omega_2 = 667\ cm^{-1}$ degenerate, $\omega_3 = 2349\ cm^{-1}$, $\omega_\perp = 410\ cm^{-1}$. For the parallel frustrated translation we estimate $\omega_\parallel = 14\ cm^{-1}$. Unpublished results for CO_2/Cu(100) show a TPD peak maximum at 100–110 K (*45*). From this we estimate a ground state energy $E_e = -463\ kJ\ mol^{-1}$. A detailed comparison with experiment is not feasible as the peak is not well separated from the peak from desorption of multilayers.

A.11. Kinetic Data

After determining the thermodynamic parameters in Section 4 we can now proceed to the determination of the kinetic parameters, i.e., the rate constants k_2, k_4, and k_7.

In the case of low conversions, low coverages, and low H_2O/CO ratio, the rate of the water gas shift reaction, Eq. (26), is reduced to

$$r = \frac{1}{2} k_2 K_1 \frac{pH_2O}{p_0}. \qquad (111)$$

From available measurements of the water gas shift reaction rate on Cu(110) and Cu(111) single crystals (*4, 10*) it is possible to get an estimate of k_2K_1. The preexponential factor A and the activation energy $E^\ddagger$ calculated from the experimental values of r have to be converted using the calculated value of K_1 to get A_2 and $E_2^\ddagger$, Eqs. (11). From the saturation coverages of O* we deduce that the number of active sites is 0.5 ML for both Cu(110) and Cu(111). Over Cu(110) slightly different parameters were found from the production of each of the two gases. In the present model these rates must be identical and the observed difference must be interpreted as experimental uncertainty. From the data for H_2 production over Cu(110) we find $E^\ddagger = 44.3\ kJ\ mol^{-1}$ and $A = 10.4 \times 10^5\ s^{-1}$ while from the production of CO_2 we find $E^\ddagger = 37.1\ kJ\ mol^{-1}$ and $A = 2.64 \times 10^5\ s^{-1}$. In the calculations we use the parameters determined from H_2 production. From the measurements over Cu(111) we find $E^\ddagger = 73.7\ kJ\ mol^{-1}$ and $A = 5.78 \times 10^7\ s^{-1}$. The shift rate is thus much higher on the Cu(110) plane than on the Cu(111) plane indicating that the shift reaction is structure sensitive. The structural sensitivity is caused by a variation in the *barrier* to dissociation of H_2O*. The contribution from differences in binding energy for H_2O* is small (Section 4). For Cu(110) we find $A_2 = 1.10 \times 10^{12}\ s^{-1}$ and $E_2^\ddagger = 93.3\ kJ\ mol^{-1}$ and for Cu(111) $A_2 = 9.90 \times 10^{13}\ s^{-1}$ and $E_2^\ddagger = 114.0\ kJ\ mol^{-1}$.

The rate constant k_7 can be determined from the dissociation probability for CO_2 on Cu. The dissociation probability for CO_2 according to the reaction

$$CO_2(g) + * \rightleftharpoons CO(g) + O* \qquad (112)$$

is 10^{-9} to 10^{-11} in the temperature range 430–612 K with an activation energy in the range 62–69 kJ/mol (*13*). These experiments on Cu(110) are thus consistent with a prefactor of 1.1×10^{-3} and an activation energy of 67 kJ mol^{-1}. From a mass balance for CO_2* a relation between the rate constant k_7 and the dissociation probability of CO_2 $\bar{\sigma}_{CO_2}$ is established:

$$rAd = \frac{P_{CO_2}}{(2\pi m k_B T)^{1/2}} A \bar{\sigma}_{CO_2} \theta*. \qquad (113)$$

A is the area of the surface, d is the density of sites, and the rate r is

$$r = \frac{k_7}{K_7 K_8} \frac{p_{CO_2}}{p_0} \theta*. \qquad (114)$$

From the experimental data we determine the prefactor $A_7 = 3.4 \times 10^{12}\ s^{-1}$ and the activation energy $E_7^\ddagger = 64\ kJ\ mol^{-1}$. These values are not quite as accurate as we would like; however, the sticking coefficient for CO_2 is very low and experiments are extremely difficult. This reaction is not very structure sensitive (*37*) on the three low in-

dex planes in the temperature range considered in the calculations, and we therefore use the same value for Cu(111) as for Cu(110).

The rate constant k_4 can be determined from the reaction probability of hydrogen atoms on an oxygenated Cu surface (*29, 37, 49–51*). An analysis based on the available data shows that the exact value of k_4 is so low that the forward shift reaction proceeds through reaction steps 2 and 3 rather than step 4.

APPENDIX B. MATHEMATICAL DETAILS

B.1. Derivation of Eq. (10)

At gas phase equilibrium the net rates of all reaction steps are zero. Substituting $r_2 = 0$, $r_4 = 0$, and $r_7 = 0$ into Eqs. (2)–(10) we obtain

$$K_2\theta_{H_2O*}\theta_* = \theta_{OH*}\theta_{H*} \tag{115}$$

$$K_4\theta_{OH*}\theta_* = \theta_{O*}\theta_{H*} \tag{116}$$

$$K_7\theta_{CO*}\theta_{O*} = \theta_{CO_2*}\theta_*. \tag{117}$$

The coverages can then be eliminated from Eqs. (2), (115), (4), (116), (6), (7), (117), and (9). Comparing the resulting equation to the conventional equilibrium equation for the gas phase,

$$K_g = \frac{p_{CO_2}p_{H_2}}{p_{H_2O}p_{CO}}, \tag{118}$$

we obtain Eq. (10).

B.2. Derivation of Eq. (14)

Experimentally step 3 is known to be fast and we have included it in the mechanism as an equilibrium. Let us for a moment think of this equilibrium as the limit $k_3 \sim \infty$ of the corresponding rate equation

$$r_3 = k_3\theta_{OH*}^2 - \frac{k_3}{K_3}\theta_{H_2O*}\theta_{O*}. \tag{119}$$

The rate r_3 is finite and well defined but r_{3+} or r_{3-} are apparently too fast to be measured. As the coverages by OH* and O* must be stationary at each point in the catalyst bed, we have

$$r_2 - 2r_3 - r4 = 0 \tag{120}$$

$$r_3 + r_4 - r_7 = 0. \tag{121}$$

From these equations we can eliminate r_3 to obtain

$$r_7 = \tfrac{1}{2}(r_2 + r_4). \tag{122}$$

Since CO_2 is only produced through steps 7 and 8, the overall rate is

$$r = r_7. \tag{123}$$

This completes the deviation of Eq. (14). From Eqs. (120) and (121) we can calculate the apparently immeasurable rate r_3

$$r_3 = \tfrac{1}{2}(r_2 - r_4). \tag{124}$$

At all conditions considered here $r_4 \sim 0$. The finite and well defined rate ($r_3 \sim r_2$) for an equilibrium step can be understood as the mass balance forcing the net rate $r_3 = r_{3+} - r_{3-}$ to be well behaved while both the forward and backward rates are high, $r_{3+}, r_{3-} \gg r_{3+} - r_{3-}$.

B.3. Derivation of Eq. (96)

If $\bar{\sigma}_{CO}$ is the reaction probability for a CO molecule hitting the surface, the number of reacting molecules per second is

$$Adr_{7+} = \frac{p_{CO}A}{\sqrt{2\pi m k_B T}}\bar{\sigma}_{CO}, \tag{125}$$

where d is the density of sites and A is the area of the surface. In the model the rate is

$$Adr_{7+} = Adk_{7+}\theta_{CO*}\theta_{O*}, \tag{126}$$

where the coverage by CO is

$$K_6\frac{P_{CO}}{P_0}\theta_* = \theta_{CO*}. \tag{127}$$

Substituting Eqs. (126) and (127) into Eq. (125) yields Eq. (96).

B.4. Derivation of Eq. (111)

In a CO + H_2O mixture at low pressures reaction 2 or 7 could be rate limiting. However, in a surplus of CO calculations show

that r_7 will be faster than r_2, and r_2 will thus be rate limiting. The relevant rate expression, Eq. 111, can easily be derived by using the corresponding equilibrium expressions for steps 4 and 7 in the derivation of the rate expression, Section 3.

Alternatively, one can determine the relevant limit, $p_{H_2} = 0$, $p_{CO} \sim 0$, $p_{CO_2} = 0$, $p_{H_2O} \sim 0$, from the general expression, Eqs. (14) and (2)–(9). The intermediate results are $\theta_{H*} = 0$, $\theta_{CO_2*} = 0$, $b \sim 0$, $c \sim 0$, $\theta_{O*} \sim 0$, $\theta_{OH*} \sim 0$ and $\theta_* \sim 1$. The final result of both derivations is evidently the same:

$$r = \frac{1}{2} k_2 K_1 \frac{p_{H_2O}}{p_0}. \qquad (128)$$

ACKNOWLEDGMENTS

Numerous discussions with B. S. Clausen and S. L. Andersen are gratefully acknowledged. Financial support from the Danish Research Councils through the Center for Surface Reactivity is gratefully acknowledged. C. T. Campbell thanks the U.S. Department of Energy, Office of Basic Energy Sciences, Chemical Sciences Division, for financial support and the Camille and Henry Dreyfuss Foundation for a Teacher–Scholar Award.

REFERENCES

1. Twigg, M. V. (Ed.), "Catalyst Handbook" (2nd ed.), Wolfe Publishing, London, 1989.
2. Newsome, D. S., *Catal. Rev. Sci. Eng.* **21,** 275 (1980).
3. Bohlbro, H., and Jørgensen, M. H., *Chem. Eng. World* **5,** 46 (1970).
4. Nakamura, J., Campbell, J. M., and Campbell, C. T., *J. Chem. Soc. Faraday Trans.* **86,** 2725 (1990).
5. Chinchen, G. C., and Jennings, J. R., Patent EP 0 296 734 A1 (to ICI).
6. Hadden, R. A., Vanderwell, H. D., Waugh, K. C., and Webb, G., *in* "Proceedings of the 9th International Congress of Catalysis, Calgary, 1988" (M. J. Phillips and M. Ternan, Eds.), Vol. 4, p. 1853, Chem. Institute of Canada, Ottawa, 1988.
7. Fiolitakis, E., and Hofman, H., *J. Catal.* **80,** 328 (1983).
8. Van Herwijnen, T., and de Jong, W. A., *J. Catal.* **63,** 83 (1980).
9. Van Herwijnen, T., "On the Kinetics and Mechanism of the CO-Shift Conversion on a Copper/Zinc Oxide Catalyst," University of Technology, Delf, 1973.
10. Campbell, C. T., and Daube, K. A., *J. Catal.* **104,** 109 (1987).
11. Grenoble, D. C., Estadt, M. M., and Ollis, D. F., *J. Catal.* **49,** 285 (1989).
12. Salmi, T., and Hakkarainen, R., *Appl. Catal.* **49,** 285 (1989).
13. Nakamura, J., Rodriguez, J. A., and Campbell, C. T., *J. Phys. Condensed Matter* **1,** SB149 (1989).
14. Hachicha, S., Hofmann, P., and Bradshaw, A. M., *in* "Proceedings, 4th ICCS and Ecoss. 3, Cannes Suppl. Le Vide, Les Couches Minces," Vol. 201, p. 498, 1980.
15. Stoltze, P., *Phys. Scr.* **36,** 824 (1987).
16. Atkins, P. W., "Physical Chemistry," 2nd ed., Oxford Univ. Press, Oxford, 1984.
17. Taylor, P. A., Rasmussed, P. B., Ovesen, C. V., Stoltze, P., and Chrokendorff, I., Formate synthesis on Cu(100), submitted for publication.
18. Boudart, M., and Djega-Mariadassou, G., "Kinetics of Heterogeneous Catalytic Reactions," Princeton Univ. Press, Princeton, NJ, 1984.
19. Press, W. H., Flannery, B. P., Teukolsky, S. A., and Vetterling, W. T., "Numerical Recipes," Cambridge Univ. Press, Cambridge, U.K. 1987.
20. Hansen, L. B., M. Sc. Thesis, Technical University of Denmark, 1990.
21. Woodruff, D. P., Hayden, B. E., Prince, K., and Bradshaw, A. M., *Surf. Sci.* **123,** 397 (1982).
22. Harendt, C., Goschnick, J., and Hirchwald, W., *Surf. Sci.* **152/153,** 453 (1985).
23. Stull, D. R., and Prophet, H. (Eds.), "JANAF Thermochemical Tables," 2nd ed., National Bureau of Standards, Washington, DC, 1971.
24. Feibelman, P. J., and Hamann, D. R., *Surf. Sci.* **173,** L582 (1986).
25. Ho, W., DiNardo, N. J., and Plummer, E. W., *J. Vac. Sci. Technol.* **17,** 134 (1980).
26. Anger, G., Winkler, A., and Rendulic, K. D., *Surf. Sci.* **220,** 1 (1989).
27. Campbell, J. M., Domagala, M. E., and Campbell, C. T., submitted for publications.
28. Hayden, B. E., and Lamont, C. L. A., *Phys. Rev. Lett.* **63,** 1823 (1989).
29. Hayden, B. E., and Lamont, C. L. A., *J. Phys. Condensed Matter* **1,** SB33 (1989).
30. Michelsen, H. A., and Auerbach, D. J., to be published.
31. Wachs, I. E., and Madix, R. J., *Surf. Sci.* **84,** 375 (1979).
32. Bange, K., Grider, D. E., Madey, T. E., and Sass, J. K., *Surf. Sci.* **136,** 38 (1984).
33. Lackey, D., Scott, J., Straehler, B., and Sass, J. K., *J. Chem. Phys.* **91,** 1365 (1989).
34. Au, C., Breza, J., and Roberts, M. W., *Chem. Phys. Lett.* **66,** 340 (1979).
35. Thiel, P. A., and Madey, T. E., *Surf. Sci. Reports* **7,** 211 (1987).
36. Mundenar, J. M., Baddorf, A. P., Plummer, E. W.,

Sneddon, L. G., Didio, R. A., and Zehner, D. H., *Surf. Sci.* **188,** 15 (1987).
37. Arlow, J. S., and Woodruff, D. P., *Surf. Sci.* **180,** 89 (1987).
38. Domagala, M. E., and Campbell, C.T., *Catal. Lett.*, in press.
39. Giamello, E., Fubini, B., Lauro, P., and Bossi, A., *J. Catal.* **87,** 443 (1984).
40. Stuve, E. M., Madix, R. J., and Sexton, B. A., *Surf. Sci.* **111,** 11 (1980).
41. Clendening, W. D., Rodriguez, J. A., Campbell, J. M., and Campbell, C. T., *Surf. Sci.* **216,** 429 (1989).
42. Nørskov, J. K., *Rep. Prog. Phys.* **53,** 1253 (1990).
43. Raval, R., Parker, S. F., Pemble, M. E., Hollins, P., Pritchard, J., and Chesters, M. A., *Surf. Sci.* **203,** 353 (1988).
44. Uvdal, P., Karlsson, P. A., Nyberg, C., and Anderson, S., *Surf. Sci.* **202,** 167 (1988).
45. Chorkendorff, I., unpublished.
46. Norton, P. R., and Tapping, R. L., *Chem. Phys. Lett.* **38,** 207 (1976).
47. Rodriquez, J. A., Clending, W. D., and Campbell, C. T., *J. Phys. Chem.* **93,** 5238 (1989).
48. Bartos, B., Freund, H-J., Kuhlembeck, M., Neumann, M., Linder, H., and Müller, K., *Surf. Sci.* **179,** 59 (1987).
49. van Pruissen, O. P., Dings, M. M. M., and Gijzeman, O. L. J., *Surf. Sci.* **179,** 377 (1987).
50. Habraken, F. H. M. P., and Bootsma, G. A., *Surf. Sci.* **87,** 333 (1979).
51. Mesters, C. M. A. M., Vink, T. J., Gijzeman, O. L. J., and Geus, J. W., *Surf. Sci.* **135,** 428 (1983).